Research Article | Vol. 26, No. 3 | 5 Feb 2018 | OPTICS EXPRESS 2817
Optics EXPRESS

Giant Goos-Hänchen shifts in non-Hermitian dielectric multilayers incorporated with graphene

DONG ZHAO,[1,2] SHAOLIN KE,[3] QINGJIE LIU,[1] BING WANG,[1,*] AND PEIXIANG LU[1,3,4]

[1]*Wuhan National Laboratory for Optoelectronics and School of Physics, Huazhong University of Science and Technology, Wuhan 430074, China*
[2]*School of Electronics Information and Engineering, Hubei University of Science and Technology, Xianning 437100, China*
[3]*Laboratory for Optical Information Technology, Wuhan Institute of Technology, Wuhan 430205, China*
[4]*lupeixiang@hust.edu.cn*
**wangbing@hust.edu.cn*

Abstract: We theoretically investigate the Goos-Hänchen (GH) shifts of optical beam in a defective photonic crystal composed of dielectric multilayers and graphene. The system is non-Hermitian and possesses exceptional points (EPs) as the scattering matrix becomes defective at the zero points of reflection. The reflective wave at EPs experiences an abrupt phase change and there the eigenvalues of scattering matrix coalesce. The GH shifts are extremely large near EPs in parametric space composed of dielectric refractive index and incident angle. The positive and negative maxima of GH shifts could be as high as 10^3 times of the incident wavelength. The direction of GH shifts switches at EPs and the EPs position can be readily controlled by the chemical potential of graphene. Moreover, the GH shifts should remarkably change as the incident waves impinge on the structure from opposite directions. The study of GH shifts in the graphene incorporated multilayers may find great applications in highly sensitive sensors.

OCIS codes: (050.2230) Fabry-Perot; (310.4165) Multilayer design; (120.5700) Reflection.

References and links

1. F. Goos and H. Hänchen, "A new and fundamental experiment on total reflection," Ann. Phys. (Leipzig) **1**(7-8), 333–346 (1947).
2. A. Aiello and J. P. Woerdman, "Role of beam propagation in Goos-Hänchen and Imbert-Fedorov shifts," Opt. Lett. **33**(13), 1437–1439 (2008).
3. A. Aiello, M. Merano, and J. P. Woerdman, "Brewster Cross Polarization," Opt. Lett. **34**(8), 1207–1209 (2009).
4. M. Merano, A. Aiello, G. W. 't Hooft, M. P. van Exter, E. R. Eliel, and J. P. Woerdman, "Observation of Goos-Hänchen shifts in metallic reflection," Opt. Express **15**(24), 15928–15934 (2007).
5. M. P. Araújo, S. A. Carvalho, and S. De Leo, "The asymmetric Goos–Hänchen effect," J. Opt. **16**(1), 015702 (2014).
6. O. J. S. Santana, S. A. Carvalho, S. De Leo, and L. E. E. de Araujo, "Weak measurement of the composite Goos-Hänchen shift in the critical region," Opt. Lett. **41**(16), 3884–3887 (2016).
7. C. Prajapati and D. Ranganathan, "Goos-Hanchen and Imbert-Fedorov shifts for Hermite-Gauss beams," J. Opt. Soc. Am. A **29**(7), 1377–1382 (2012).
8. A. Aiello, "Goos-Hänchen and Imbert-Federov shifts: a novel perspective," New J. Phys. **14**(1), 013058 (2012).
9. K. Y. Bliokh and A. Aiello, "Goos-Hänchen and Imbert-Fedorov beam shifts: an overview," J. Opt. **15**(1), 014001 (2013).
10. M. P. Araujo, S. De Leo, and G. G. Maia, "Closed–form expression for the Goos-Hänchen lateral displacement," Phys. Rev. A **93**(2), 023801 (2016).
11. M. Merano, A. Aiello, M. P. van Exter, and J. P. Woerdman, "Observing angular deviations in the specular reflection of a light beam," Nat. Photonics **3**(6), 337–340 (2009).
12. M. P. Araujo, S. A. Carvalho, and S. De Leo, "Maximal breaking of symmetry at critical angle and closed-form expression for angular deviations of the Snell law," Phys. Rev. A **90**(3), 033844 (2014).
13. G. Jayaswal, G. Mistura, and M. Merano, "Observing angular deviations in light-beam reflection via weak measurements," Opt. Lett. **39**(21), 6257–6260 (2014).

#315272 https://doi.org/10.1364/OE.26.002817
Journal © 2018 Received 8 Dec 2017; revised 20 Jan 2018; accepted 22 Jan 2018; published 25 Jan 2018

Optics EXPRESS

14. M. P. Araujo, S. De Leo, and G. G. Maia, "Optimizing Weak Measurements to Detect Angular Deviations," Ann. Phys. (Berlin) **529**(9), 1600357 (2017).
15. A. Aiello, M. Merano, and J. P. Woerdman, "Duality between spatial and angular shift in optical reflection," Phys. Rev. A **80**(6), 061801 (2009).
16. H. M. Lai and S. W. Chan, "Large and negative Goos-Hänchen shift near the Brewster dip on reflection from weakly absorbing media," Opt. Lett. **27**(9), 680–682 (2002).
17. L. G. Wang, H. Chen, and S. Y. Zhu, "Large negative goos-hänchen shift from a weakly absorbing dielectric slab," Opt. Lett. **30**(21), 2936–2938 (2005).
18. B. Zhao and L. Gao, "Temperature-dependent Goos-Hänchen shift on the interface of metal/dielectric composites," Opt. Express **17**(24), 21433–21441 (2009).
19. J. C. Martinez and M. B. A. Jalil, "Theory of giant Faraday rotation and Goos-Hänchen shift in graphene," Europhys. Lett. **96**(2), 27008 (2011).
20. M. Merano, "Optical beam shifts in graphene and single-layer boron-nitride," Opt. Lett. **41**(24), 5780–5783 (2016).
21. B. M. Jost, A. A. R. Al-Rashed, and B. E. Saleh, "Observation of the Goos-Hänchen effect in a phase-conjugate mirror," Phys. Rev. Lett. **81**(11), 2233–2235 (1998).
22. L. G. Wang and S. Y. Zhu, "Giant lateral shift of a light beam at the defect mode in one-dimensional photonic crystals," Opt. Lett. **31**(1), 101–103 (2006).
23. J. He, J. Yi, and S. He, "Giant negative Goos-Hänchen shifts for a photonic crystal with a negative effective index," Opt. Express **14**(7), 3024–3029 (2006).
24. S. Longhi, G. Della Valle, and K. Staliunas, "Goos-Hänchen shift in complex crystals," Phys. Rev. A **84**(4), 042119 (2011).
25. M. Abbas and S. Qamar, "Amplitude control of the goos-hänchen shift via a kerr nonlinearity," Laser Phys. Lett. **11**(1), 5201 (2013).
26. Z. Hong, Q. Zhang, S. A. Rezvani, P. Lan, and P. Lu, "Tunable few-cycle pulses from a dual-chirped optical parametric amplifier pumped by broadband laser," Opt. Laser Technol. **98**, 169–177 (2018).
27. Y. L. Chuang and R. K. Lee, "Giant Goos-Hänchen shift using PT symmetry," Phys. Rev. A **92**(1), 013815 (2015).
28. P. Ma and L. Gao, "Large and tunable lateral shifts in one-dimensional PT-symmetric layered structures," Opt. Express **25**(9), 9676–9688 (2017).
29. C. M. Bender and S. Boettcher, "Real spectra in non-Hermitian Hamiltonians having PT symmetry," Phys. Rev. Lett. **80**(24), 5243–5246 (1998).
30. C. E. Rüter, K. G. Makris, R. El-Ganainy, D. N. Christodoulides, M. Segev, and D. Kip, "Observation of parity–time symmetry in optics," Nat. Phys. **6**(3), 192–195 (2010).
31. Z. Lin, H. Ramezani, T. Eichelkraut, T. Kottos, H. Cao, and D. N. Christodoulides, "Unidirectional invisibility induced by PT-symmetric periodic structures," Phys. Rev. Lett. **106**(21), 213901 (2011).
32. Y. D. Chong, L. Ge, and A. D. Stone, "PT-symmetry breaking and laser-absorber modes in optical scattering systems," Phys. Rev. Lett. **106**(9), 093902 (2011).
33. V. V. Konotop, V. S. Shchesnovich, and D. A. Zezyulin, "Giant amplification of modes in parity-time symmetric waveguides," Phys. Lett. A **376**(42-43), 2750–2753 (2012).
34. L. Feng, Y. L. Xu, W. S. Fegadolli, M. H. Lu, J. E. B. Oliveira, V. R. Almeida, Y. F. Chen, and A. Scherer, "Experimental demonstration of a unidirectional reflectionless parity-time metamaterial at optical frequencies," Nat. Mater. **12**(2), 108–113 (2013).
35. L. Feng, X. Zhu, S. Yang, H. Zhu, P. Zhang, X. Yin, Y. Wang, and X. Zhang, "Demonstration of a large-scale optical exceptional point structure," Opt. Express **22**(2), 1760–1767 (2014).
36. D. Zhao, Z. Q. Wang, H. Long, K. Wang, B. Wang, and P. X. Lu, "Optical bistability in defective photonic multilayers doped by graphene," Opt. Quantum Electron. **49**(4), 163 (2017).
37. S. Ke, B. Wang, H. Long, K. Wang, and P. Lu, "Topological mode switching in a graphene doublet with exceptional points," Opt. Quantum Electron. **49**(6), 224 (2017).
38. H. Huang, S. Ke, B. Wang, H. Long, K. Wang, and P. Lu, "Numerical study on plasmonic absorption enhancement by a rippled graphene sheet," J. Lightwave Technol. **35**(2), 320–324 (2017).
39. C. Qin, B. Wang, H. Long, K. Wang, and P. Lu, "Nonreciprocal phase shift and mode modulation in dynamic graphene waveguides," J. Lightwave Technol. **34**(16), 3877–3883 (2016).
40. S. Ke, B. Wang, C. Qin, H. Long, K. Wang, and P. Lu, "Exceptional points and asymmetric mode switching in plasmonic waveguides," J. Lightwave Technol. **34**(22), 5258–5262 (2016).
41. Q. Liu, B. Wang, S. Ke, H. Long, K. Wang, and P. Lu, "Exceptional points in Fano-resonant graphene metamaterials," Opt. Express **25**(7), 7203–7212 (2017).
42. X. F. Zhu, "Defect states and exceptional point splitting in the band gaps of one-dimensional parity-time lattices," Opt. Express **23**(17), 22274–22284 (2015).
43. S. L. Wang, B. Wang, C. Z. Qin, K. Wang, H. Long, and P. X. Lu, "Rabi oscillations of optical modes in a waveguide with dynamic modulation," Opt. Quantum Electron. **49**(11), 389 (2017).
44. S. Thongrattanasiri, I. Silveiro, and G. D. A. F. Javier, "Plasmons in electrostatically doped graphene," Appl. Phys. Lett. **100**(20), 201105 (2012).
45. M. Merano, "Fresnel coefficients of a two-dimensional atomic crystal," Phys. Rev. A **93**(1), 013832 (2016).

Optics EXPRESS

1. Introduction

Since the Goos-Hänchen (GH) shift was first observed experimentally by Goos and Hänchen in 1947 [1], many efforts have been devoted into the theoretical and experimental studies of the effect [2–10]. The GH shift may manifest a spatial or angular shift [11–14], which could occur individually or simultaneously at the interface of two materials with different permittivities [15]. GH shifts have been reported in various systems, including dielectric slab [16, 17], metamaterials [18], graphene [19, 20], phase-conjugate mirrors [21], and photonic crystals (PCs) [22–24]. In order to enhance the GH effect, one has utilized the Kerr nonlinearity [25, 26] and fabricated defect layers in PCs [22]. Recently, a giant enhancement of GH shift has been achieved in the parity-time (PT)-symmetry cavity [27]. It has also been reported that GH shifts should be large inside the reflection band and became extremely large at exceptional points (EPs) in PT-symmetric photonic crystals [24]. Simultaneously, very large GH shifts may exist in periodic dielectric multilayers with PT-symmetry where the lateral shifts are tightly independent on the incident direction [28].

Although the PT-symmetry stems from the quantum system [29], it could find a counterpart in optics balanced gain and loss, i.e., $n(\mathbf{r}) = n^*(\mathbf{r})$ [30]. In an open quantum system, non-Hermitian Hamiltonian with PT symmetry can exhibit real eigenvalues as well. But the eigenvalues and eigenfunctions of the Hamiltonian coalesce at EPs, known as PT-symmetry breaking points. The PT-symmetry system has many unique optical features, and found applications in unidirectional invisibility [31], coherent perfect laser absorbers [32], and giant wave amplification [33].

In fact, the two conditions of both non-Hermiticity and PT-symmetry to form EPs are not necessary for the same time. The lossy metamaterials are non-Hermitian and could also be utilized to yield EPs [34]. Since giant GH shifts are present in PT-symmetry and notable at EPs [24, 27, 28], it is necessary to explore the behavior of GH shifts in non-Hermitian systems. Through the unique characteristic of EPs including unidirectional zero reflection and abrupt phase change, we could also in turn find EPs in non-Hermitian systems [35]. Recently, graphene has been widely employed to realize many optoelectronic functionalities for its unique optical, electronic, and mechanical properties [36–39]. Graphene is a lossy material due to the limited relaxation time of electrons. As a result, incorporating the graphene into metamaterials can constitute a non-Hermitian system [40, 41], in which EPs locate at the zero points of reflection [24, 42] and the EPs positions in parametric space can be tuned by the chemical potential of graphene.

In this work, we incorporate graphene in dielectric multilayer to construct a non-Hermitian system and investigate the spatial GH shift of reflected light beam from the multilayer. Although the GH shift in a single layer of two-dimensional material like graphene or boron-nitride has been explored, the shift is demonstrated to be extremely small [20]. Here we show that the GH shift in a bulk multilayer structure and the incorporated graphene plays the role to realize non-Hermiticity of the system. The multilayers are constituted by periodic dielectric layers with a defect in the center of the structure. The reflectance is direction-dependent as light is incident from two sides of opposite directions. The field distribution for defective mode is provided to account for large GH shifts in following study. Then, we find two EPs existing in the parameter space composed of dielectric refractive index and incident angle. The EPs are confirmed through the unique properties, including eigenvalue coalescence and abrupt phase change [40, 41]. We also discuss the GH shifts and their polarity, the singularity at EPs, and the direction-dependence of GH shifts. Especially, the differences in GH shifts with the cases in PT-symmetry multilayers [28] are especially concerned. We further explore the control of EPs in the parameter space by changing the graphene chemical potential. Numerical simulations show that the incident beam width has effect on GH shifts [22]. In the end, we illustrate the application of GH shifts in dielectric refractive index sensing.

Optics EXPRESS

2. Non-Hermitian dielectric multilayers

The structure of the dielectric multilayers incorporated with graphene is shown in Fig. 1. The multilayers stack forms a Fabry-Pérot cavity with Bragg gratings. The layers A and B represent the dielectrics with different refractive indices and they are alternatively arranged along the Z-axis, forming the Bragg gratings on two sides of a photonic crystal (PC) defect. The single-layer graphene C is embedded in the middle of the cavity. The right-terminal layer of the PC is replaced by the dielectric D so as to break the geometric symmetry. The dielectric refractive index of layer D is tunable which can be achieved by dynamic modulations [43]. The layers A, B, and D have the same thickness. The optical thicknesses of layers are near quarter-wavelength $n\lambda/4$, where λ denotes the free space wavelength of incident waves.

The incident plane wave is obliquely projected at an angle of θ into the dielectric multilayers. The transmission coefficients on both sides (the left and the right) of the reciprocal system are the same and represented by t. But the reflection coefficients at the left and right sides should be different and denoted by r_1 and r_2, respectively. The reflection coefficients and transmission coefficients could be obtained by the transfer matrix method (TMM).

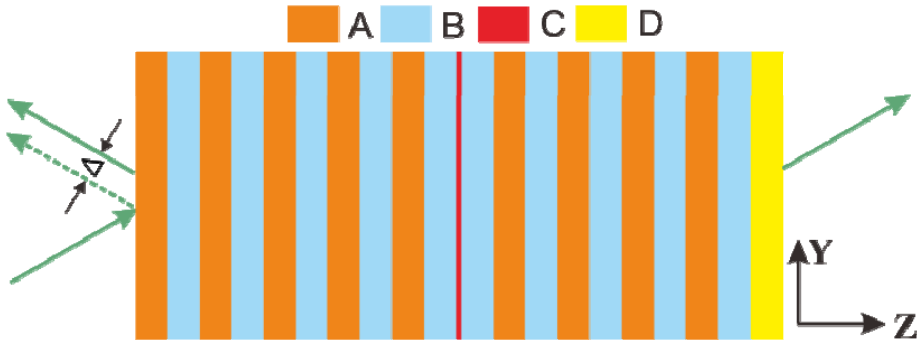

Fig. 1. Schematic of non-Hermitian dielectric multilayers. For the primitive unit-cell layer A, B, graphene C and dielectric D, the thicknesses are d = 0.2 μm and the graphene thickness d_c = 1 nm. The refractive indices of dielectrics A and B are n_a = 2.2, n_b = 1.8 and $n_d = n' + in''$ with n'' = 0.05.

The scattering matrix for incident and scattered waves in the structure can be expressed as [24, 42]

$$S = \begin{bmatrix} t & r_1 \\ r_2 & t \end{bmatrix} \tag{1}$$

where r_1, r_2 represent the reflection coefficients and t is the transmission coefficient. As $r_{1,2} = |r_{1,2}|\exp(i\varphi_{1,2})$, the GH shifts of reflected beams can read [28]

$$\Delta_{1,2} = -\frac{\lambda}{2\pi}\frac{d\varphi_{1,2}}{d\theta}, \tag{2}$$

where $\varphi_{1,2}$ are the phases of reflection coefficients $r_{1,2}$. As the structure is lossy and the geometry is asymmetric, the S-matrix has to be non-Hermitian. The eigenvalues and eigenvectors of S-matrix are $\beta_{1,2} = t \pm (r_1 r_2)^{1/2}$ and $(r_1^{1/2}, \pm r_2^{1/2})$, respectively. The two physical quantities coalesce at $(r_1 r_2)^{1/2} = 0$, that is, the EPs of the eigenvalues. In other words, the EPs appear as either r_1 or $r_2 = 0$. Based on the definition of reflectance $R_{1,2} = |r_{1,2}|^2$, we could derive the condition for realizing EPs, making R_1 or $R_2 = 0$. As $R_1 R_2 = 0$, the related reflection phase φ_1 or φ_2 has to experience a dislocation, which is a unique property of EPs. The zero reflection and phase dislocation can be utilized to seek out EPs. Since the structure

in Fig. 1 is asymmetric, it is hard to make both R_1 and R_2 be zero simultaneously. Consequently, there are two EPs with new characteristics.

3. EPs in non-Hermitian multilayers

For transverse electric (TE) wave, now we study the reflectance and transmittance of the structure when light is injected from the left side. In the simulation, graphene is treated as a thin film with an equivalent thickness d_g, then, the relative equivalent permittivity of graphene could be given by $\varepsilon_g = 1 + i\sigma_g\eta_0/(k_0 d_g)$ [36, 39], where η_0 is the vacuum resistivity and σ_g is the surface conductivity of graphene. The surface conductivity of graphene can be modeled using Kubo formula [44], which depends on the incidence wavelength λ, chemical potential μ_c, relaxation time τ, and absolute temperature T. Although the treatment of equivalent thickness for graphene is based on theoretical approximation, the optical response of graphene can be accurately featured as long as the equivalent thickness is small enough, typically smaller than 1 nm [36–38, 45].

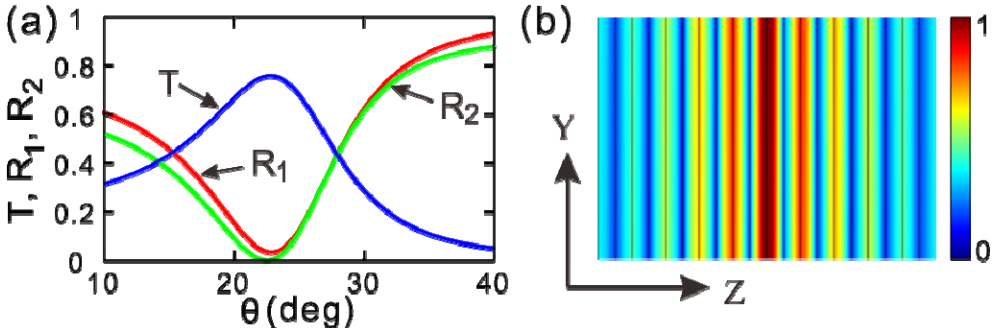

Fig. 2. (a) The calculated spectra of T (the blue curve), R_1 (the red curve) and R_2 (the green curve) as a function of incident angle θ for dielectric refractive index $n' = 2.0$. R_1 and R_2 are the reflectance of light incident from the left and right, respectively. (b) Electric fields intensity ($|E_z|^2$) distribution of defective mode.

Figure 2(a) shows the reflection and transmittance as a function of the incident angle θ. The reflectance spectra reach the minimum values of $R_1 = 0.034$ and $R_2 = 0.001$ at $\theta = 22.89°$ and $\theta = 22.57°$, respectively. As a result, the angular GH shift should be very small since the slop of reflectance approaches to zero near the minimum [15]. The difference of the two curves indicates that the reflectance is asymmetric and dependents on the incident direction. Comparably, the transmittance from opposite incident direction is reciprocal. The maximum transmittance reaches $T = 0.76$ at $\theta = 22.05°$. The peak at the spectrum is aroused by the defect mode in the multilayers. Figure 2(b) illustrates the electric field distribution of the defect mode along the z-axis. It shows that most of the power is tightly confined at the interface of the defect and the field exponentially decays as departing from the center. The incident wavelength is set to $\lambda = 1.55$ μm. Other parameters are chosen as $d_g \approx 0.3$ nm [38, 39], $\mu_c = 0.5$ eV, and $\tau = 0.5$ ps.

Now we focuse on the EPs in the system. Figure 3(a) illustrates the reflectance R_1 as a function of the incident angle and dielectric refractive index for light incident from the left side of the structure. One sees that there is a nadir locating at $\theta = 23.978°$ and $n' = 2.316$. The nadir value is as low as $R_1 = 2.972 \times 10^{-8}$, which equals nearly to zero considering the limit of calculation accuracy. Figure 3(b) plots the real and imaginary parts of eigenvalues of the scattering matrix vary with the incident angle as $n' = 2.316$. One sees that Re($\beta_{1,2}$) and Im($\beta_{1,2}$) almost coalesce as the reflection approaches to zero, validating the appearance of EPs. The EP location is denoted by EP_1 in parametric space with $\theta_{EP1} = 23.978°$ and $n_{EP1} = 2.316$. For light incident from opposite direction of the right side, the nadir value becomes $R_2 = 1.618 \times 10^{-8}$ at $\theta_{EP2} = 22.978°$ and $n_{EP2} = 2.101$, corresponding to EP_2 as shown in Fig. 3(c).

Optics EXPRESS

The eigenvalues also degenerate at EP_2 as shown in Fig. 3(d) and the levels of Re($\beta_{1,2}$) and Im($\beta_{1,2}$) experience crossing and anti-crossing in the vicinity of the two EPs [40].

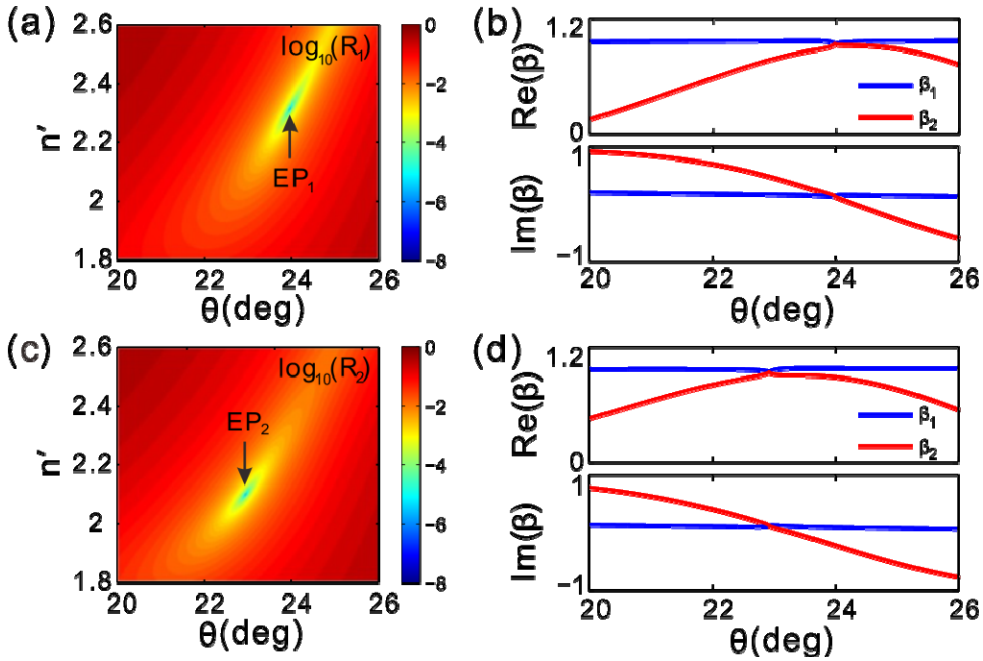

Fig. 3. (a) Reflection spectra R_1 in parametric space of incident angle and dielectric refractive index. EP_1 locating at θ_{EP1} = 23.978° and n_{EP1} = 2.316. (b) Real part and imaginary part of eigenvalues for scattering matrix vary with incident angle as $n' = n_{EP1}$. (c) Reflection spectra R_2 and EP_2 locating at θ_{EP2} = 22.978° and n_{EP2} = 2.101. (d) Real part and imaginary part of eigenvalues for scattering matrix as $n' = n_{EP2}$. The black arrows point to the positions of EPs in (a) and (c). Light is incident from the left for (a) and (b), while incident from the right for (c) and (d).

4. GH shifts in the vicinity of EPs

The spatial GH shift relates to the phase of reflection coefficient and is proportional to the slope of reflection phase in accordance with Eq. (2). Figure 4(a) illustrates the reflection phase φ_1 in parametric space, where the dielectric refractive index and incident angle can be modified in the vicinity of EP_1. There is a phase dislocation around EP_1, which is unique for EPs in non-Hermitian systems [38]. The singularity of phase indicates that the phase should abruptly change once the parameters undergo a little variation. Figure 4(b) plots the reflection phase versus the incident angle for several sampling dielectric refractive indices. There is a hop point in the phase curve as $n' = 2.308$ and the phase difference is -2π. Neglecting the meaningless phase difference at the hop point, the curve is actually continuous with a positive slope. The phase change can approximately reach to π in a phase variation range around θ_{EP1} as the dielectric refractive index $n' < n_{EP1}$. The phase experiences a π abruptly jump at θ_{EP1} as $n' = n_{EP1}$. Comparably, the phase change can nearly reach to $-\pi$ around θ_{EP1} with a negative slope as $n' > n_{EP1}$. For light incident from the right, as depicted in Fig. 4(c), there is also a phase dislocation existing in the vicinity of EP_2. Contrary to φ_1, the hop points lie in the upper region of parametric space, corresponding with higher refractive indices. Figure 4(d) plots the reflection phase varies with the incident angle for several different dielectric refractive indices around EP_2. An abrupt phase change also occurs as $n' = n_{EP2}$. A π phase roughly climbs in a variation range of dielectric refractive index about n_{EP2} as $n' < n_{EP2}$, but a π phase drops as $n' > n_{EP2}$. The slope of phase curve is larger as n' is closer to $n_{EP1,2}$ and reaches the positive and negative maxima at EPs. Otherwise, the slope of curve can be negative or positive and the

Optics EXPRESS

polarity converts as the dielectric refractive index approaches to $EP_{1,2}$ along the same direction, indicating the direction-dependence of GH shifts, which will be studied shortly.

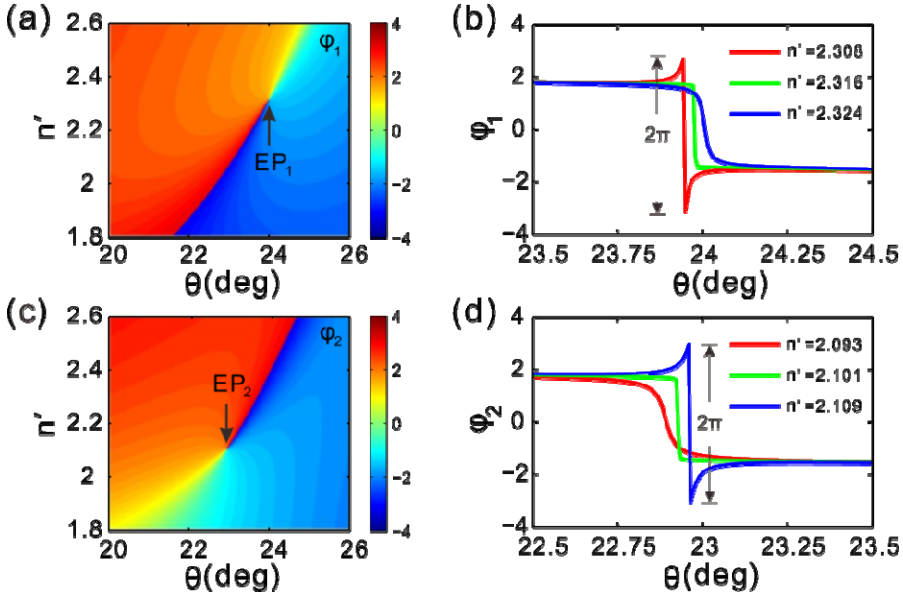

Fig. 4. (a) Phase of reflection coefficient in the vicinity of EP_1. (b) Phase curve versus incident angle for several specific refractive indices around EP_1. (c) Phase of reflection coefficient in the vicinity of EP_2. (d) Phase curve versus incident angle for several specific refractive indices around EP_2. Light is incident from the left for (a) and (b), while incident from the right for (c) and (d).

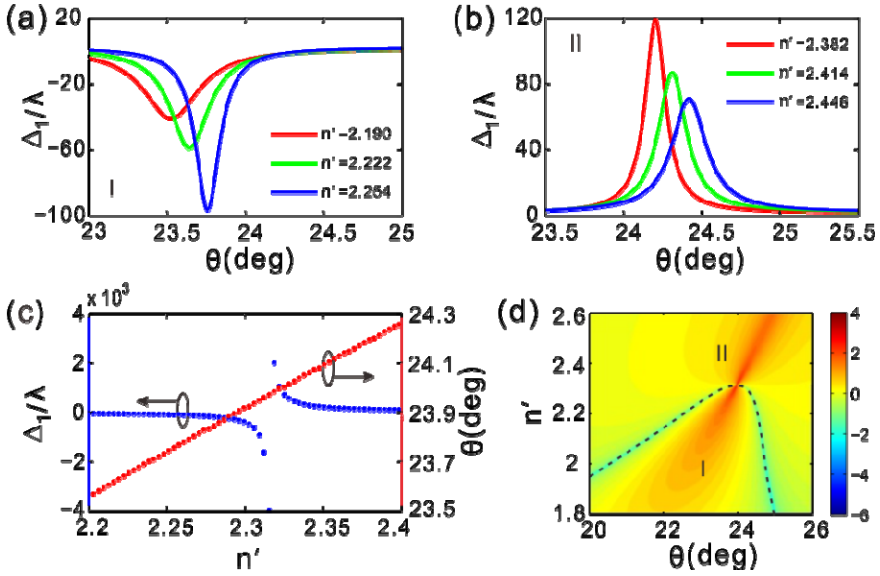

Fig. 5. (a) GH shifts versus incident angle for dielectric refractive index $n' < n_{EP1}$. (b) GH shifts versus incident angle for dielectric refractive index $n' > n_{EP1}$. (c) Maxima of GH shifts varying with dielectric refractive index around n_{EP1} (in blue dot line). Incident angle of position in parametric space for maxima versus dielectric refractive index (in red dot line). (d) GH shifts in the vicinity of EP_1. The GH shifts are negative in the part I, while positive in the part II. It has rescaled the results by taking logarithm $\log_{10}|\Delta_1/\lambda|$ for clarity.

Optics EXPRESS

The GH shift is proportional to the slope of phase curve in accordance with Eq. (2). For light incident from the left, as shown in Fig. 5(a), the GH shifts vary with the incident angle. One sees that the GH shifts are negative and a valley appears in each curve, corresponding to the dielectric refractive indices $n' = 2.190$, 2.222 and 2.254 which are below $n_{EP1} = 2.316$. It should be mentioned that, for a two-dimensional material, it may find that the negative GH shift is smaller than positive GH shift [20]. However, the situation should be different for bulk material. Here the multilayer structure behaves more like a bulk material and the defect cavity will enhance the confinement of light. The giant negative GH shift results from the permeating of electric field deeply into the multilayer. Actually, the large negative GH shift is common and has been reported in other multilayer structures [28]. For larger dielectric refractive indices, such as $n' = 2.382$, 2.414 and 2.446, the peaks emerge as shown in Fig. 5(b). As the dielectric refractive indices are closer to n_{EP1}, the corresponding curves become narrower and sharper (or deeper). Figure 5(c) displays the position of the maximum GH shift can be modified by the dielectric refractive index. The incident angle of the maxima position almost increases linearly with the dielectric refractive index, which may results from the influence of the dielectric refractive index on the reflection. Besides, the maxima of GH shifts can be negative or positive and separated by EP_1. Their absolute values sharply climb as the dielectric refractive index approaches to n_{EP1}. In the vicinity of EP_1, the negative maximum GH shift can reach as high as –4000 times of the incident wavelength, while the positive maximum can approach to 2000 times. Figure 5(d) depicts the GH shift as a function of the dielectric refractive index and incident angle. The area concerned in the parametric space is divided into two parts labeled by I and II, respectively. The GH shift is negative in part I, while it is positive in part II. The GH shift becomes zero along the dotted curve except for EP_1, at which the polarity of GH shifts converts, manifesting the singularity.

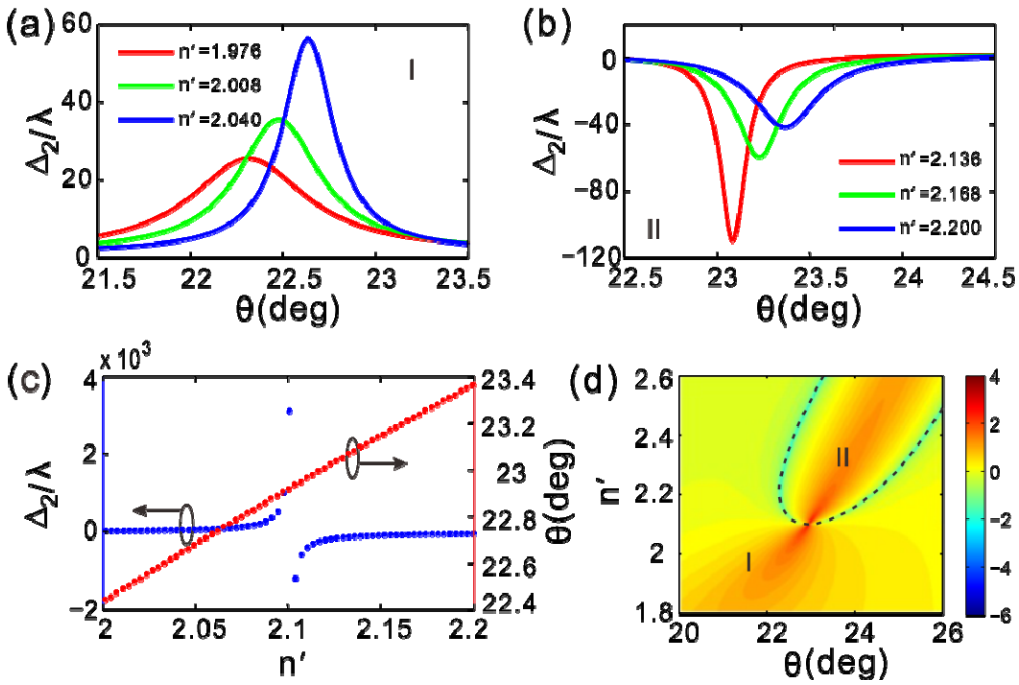

Fig. 6. (a) GH shifts versus incident angle for dielectric refractive index $n' < n_{EP2}$. (b) GH shifts versus incident angle for dielectric refractive index $n' > n_{EP2}$. (c) Maxima of GH shifts varying with dielectric refractive index around n_{EP2} (in blue dot line). Incident angle of position in parametric space for maxima versus dielectric refractive index (in red dot line). (d) GH shifts in the vicinity of EP_2. The GH shifts are positive in the part I, while negative in the part II. It has rescaled the results by taking logarithm $\log_{10}|\Delta_2/\lambda|$ for clarity.

Optics EXPRESS

For light incident from the right, as shown in Fig. 6(a), the GH shifts vary with the incident angle. The chosen dielectric refractive indices, including $n' = 1.976$, 2.008 and 2.040, are lower than $n_{EP2} = 2.101$. However, the profile of curves is similar to the case as light impinges from the left for $n' > n_{EP2}$. For larger dielectric refractive indices $n' = 2.136$, 2.168 and 2.200, as shown in Fig. 6(b), the GH shifts curves change with the incident angle, similar to the profile for light incident from the left as $n' < n_{EP2}$. The property manifests that the GH shifts are direction-dependent. In the vicinity of EP_2, the maxima of GH shifts are also divided by n_{EP2} and can reach to $\pm 10^3$ times of incident wavelength as shown in Fig. 6(c). The polarity converts at EP_2, indicating the singularity of GH shifts. Figure 6(d) shows the values are positive in part I and negative in part II. Compared with EP_1, the positive and negative positions in parametric space have been turned over. Similarly, the GH shifts are zero along the dotted curve except for EP_2.

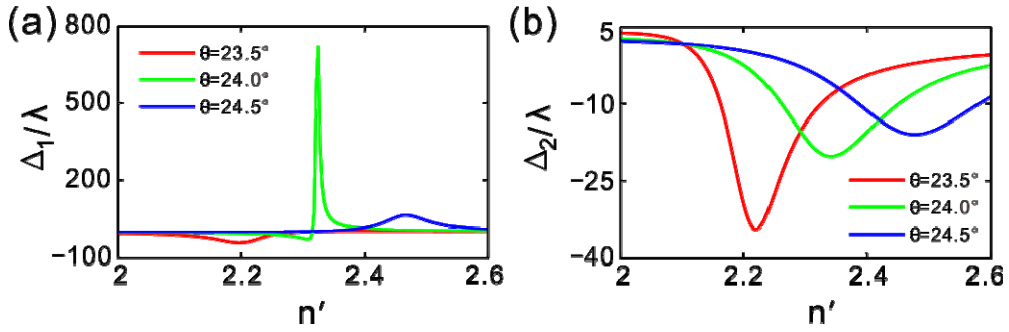

Fig. 7. (a) GH shifts versus dielectric refractive index for light incident from the left. (b) GH shifts versus dielectric refractive index for light incident from the right. The curves are in red, green and blue corresponding to incident angles $\theta = 23.5°$, 24.0° and 24.5°, respectively.

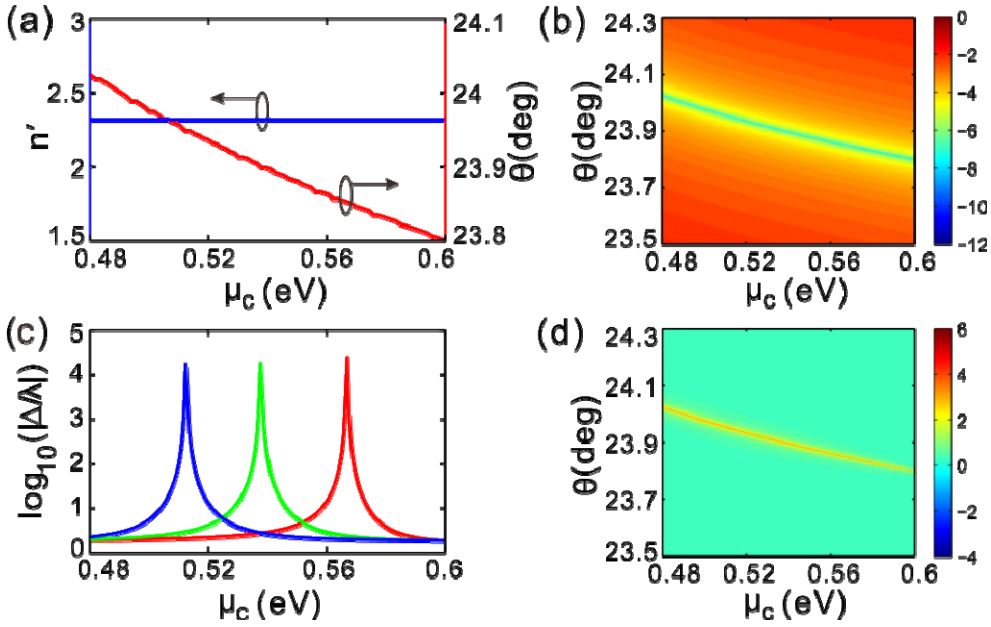

Fig. 8. (a) Position of zero-reflectance point modifying by graphene chemical potential in parametric space of incident angle and refractive index. Light is incident from the left. Refractive index is shown in blue and incident angle is shown in red. (b) Reflectance varying with incident angle and chemical potential. (c) GH shifts versus graphene chemical potential for three incident angles of $\theta = 23.85°$ (in red), 23.90° (in green) and 23.95° (in blue). (d) GH

Optics EXPRESS

shifts in parametric space of incident angle and chemical potential. The refractive index $n' = 2.316$ and it has rescaled the values by taking logarithm for clarity in (b)-(d).

In order to confirm the direction-dependence of GH shifts, we choose $\theta = 23.5°$, 24.0° and 24.5°. The three angles are distributed on both sides of $\theta_{EP1} = 23.978°$ but larger than $\theta_{EP2} = 22.978°$. For light incident from the left at a fixed incident angle, as shown in Fig. 7(a), the GH shifts vary with the dielectric refractive index. The curve has a valley as the incident angle $\theta = 23.5°$, but it has a peak as $\theta = 24.0°$ and 24.5°. For the incident angle $\theta = 24.0°$, which is closer to θ_{EP1}, the peak is sharper than the one for $\theta = 24.5°$. For light incident from the right, as shown in Fig. 7(b), the GH shifts change with the dielectric refractive index. A valley arises in each curve, and the valley becomes deeper as the incident angle more approaches to θ_{EP2}. On the whole, the peak and valley positions are identical for $\theta = 24.5°$, attributed to the fields most deeply penetrating into the multilayers at these points. The property shows the reflection is different for light impinging upon the device, so it may find potentials used for optical switches.

The EPs position can be controlled by the graphene chemical potential. In the parametric space composed of incident angle and dielectric refractive index, as shown in Fig. 8(a), the position of the zero-reflectance varies with the graphene chemical potential for light incident from the left. Changing the chemical potential from $\mu_c = 0.48$ to 0.60 eV, the dielectric refractive index remains constant at $n' = 2.316$, while the incident angle decreases with the chemical potential. Accordingly, maintaining the dielectric refractive index $n' = 2.316$, one can see lots of continuous zero-reflectance points corresponding to EPs, as shown in Fig. 8(b). Therefore, in the parametric space composed of incident angle and chemical potential, the position of EPs varies with the graphene chemical potential. This is because the surface conductivity of graphene is a function of μ_c, affecting the reflection of light. Figure 8(c) plots the GH shifts versus the chemical potential as $\theta = 23.85°$, 23.90° and 23.95°. The peaks arise in these curves and the maxima are notable. The peaks have the same values and up to 10^4 times of incident wavelength around EPs. The EPs are also singular points for GH shifts. Figure 8(d) illustrates the maxima of GH shifts go along the zero-reflective points where EPs locate in parametric space of incident angle and chemical potential.

5. GH shifts for sensing

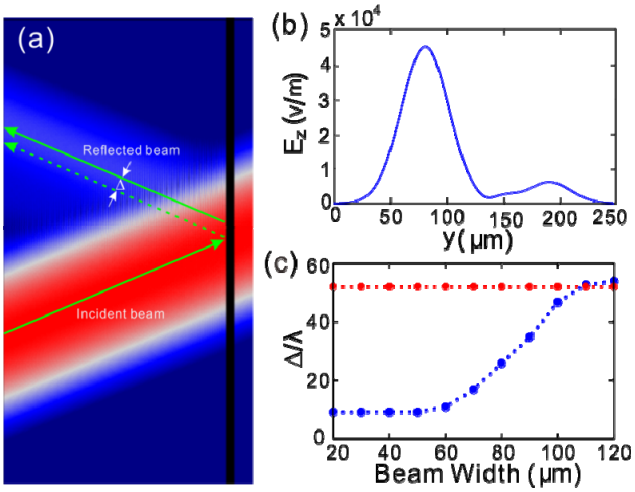

Fig. 9. (a) Electric field amplitude distribution of Gaussian beam with a finite width as $\theta = 24.8°$ and $n' = 2.46$. (b) Profile of electric field at the incident interface. (c) Influence of width on GH shifts for Gaussian beam as $\theta = 22.3°$ and $n' = 2.29$. Simulation of GH shifts for Gaussian beam with different widths (in blue dotted line) and result predicted in theory (in red dotted line).

Optics EXPRESS

As a Gaussian beam with finite width incident upon the dielectric multilayers at an angle θ from the left side, the distribution of electric field intensity in the calculating region, as shown in Fig. 9(a). Numerical simulations are performed with the commercial software COMSOL Multiphysics based on the finite element method. It shows that the reflective beam has a positive lateral shift from the position predicted by geometrical optics. For the reflected beam much weaker than the incident, we have rescaled the field by taking logarithm. Figure 9(b) gives the profile of the electric field at the incident interface, where the two peaks denote the central points of the incident and reflective beams, respectively. The GH shifts can be derived in accordance with incident angles, propagating distances and central positions of beams. The simulation result $\Delta = 12\lambda$ is lower the theoretical value $\Delta = 14\lambda$ as $\theta = 24.8°$ and $n' = 2.46$. The difference results from the influence of the Gaussian beams width on simulations. Increasing the width of Gaussian beam, the two results are satisfied well as shown in Fig. 9(c). The width effect is more obvious for larger GH shifts, while the corresponding reflection is much weaker. Here, we choose $\theta = 22.3°$ and $n' = 2.29$ on account of those factors such as reflection and the value of GH shift comprehensively. Simulations demonstrate that the GH shift can achieve $\Delta = 51\lambda$ in theory as long as the beam width surpasses 70 times of incident wavelength, which agrees with the conclusions mentioned in defective photonic crystals [22].

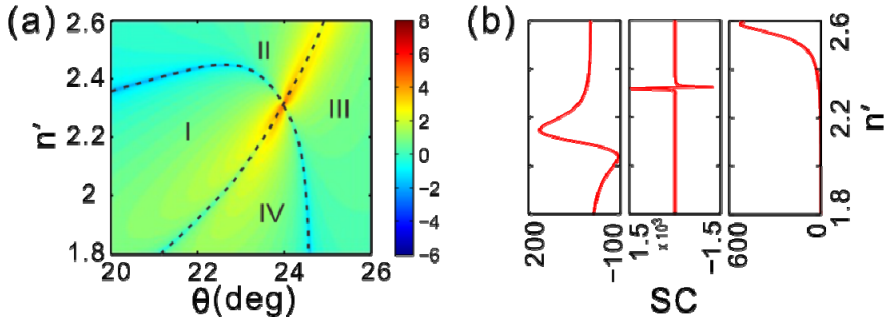

Fig. 10. (a) Sensitivity coefficient of GH shifts in parametric space of dielectric refractive index and incident angle around EP_1. It has rescaled the values by taking logarithm $\log_{10}|d\Delta/(\lambda dn')|$ for clarity. (b) Sensitivity coefficient of GH shifts tuned by dielectric refractive index at incident angles $\theta = 23°$, 24° and 25°, respectively.

The GH shift is related largely to the dielectric refractive index and is direction-dependent, so the proposed structure can be utilized for sensors or optical switches. Sensitivity coefficient (SC) is defined as the differential of GH shift changes over dielectric refractive index. For light injected from the left, not only GH shift, but also the SC is sensitive to the dielectric refractive index and incident angle as shown in Fig. 10(a), so the sensitivity of sensors possesses flexible tunability. In the vicinity of EP_1, the area is separated into four parts by the dotted lines. The values are positive in parts I and III, while they are negative in parts II and IV. The values are zero along the dotted lines except for EP_1, which is a singular point for the SC. The polarity of SC converts at EP_1 and the positive and negative maxima of SC can reach 1.3×10^6 and -1.1×10^6, respectively. Figure 10(b) shows that the SC of GH shifts can be modified by the dielectric refractive index. Here we choose three incident angles $\theta = 23°$, 24°and 23.5°, which locate at the two sides of $\theta_{EP1} = 23.978°$, respectively. A peak and a valley exist in each curve at the incident angles $\theta = 23°$ and 23.5°, while only a peak appears at $\theta = 24°$. As the incident angle moves closer to θ_{EP1}, the peak and valley become sharper and narrower. The SC represents the sensitivity of sensors in detecting physical quantities, so the devices can be used for sensitive detectors. In the study we implement sensing by employing spatial GH shift since the EPs are mainly considered. Moreover, the angular GH shift might also find interesting application in sensors.

Optics EXPRESS

6. Conclusion

In conclusion, we construct a non-Hermitian system by dielectric multilayers and graphene, which is lossy and asymmetric. The reflection property in optics is direction-dependent for light incident from the left and right. The EPs locates at zero points of reflectance. The eigenvalues of S-matrix coalescence and phase abruptly changes at EPs. In the vicinity of EPs, the GH shifts can be positive and negative and can reach as high as 10^3 times of incident wavelength. The polarity of GH shift converts at EPs which has a singularity for GH shift. Moreover, the EPs position can be controlled by the graphene chemical potential. The simulations fairly coincide with the theoretical analysis for Gaussian beam. The GH shifts are direction-dependent and sensitive to a tiny dielectric refractive index variation, so the devices have potential used for optical switches or sensors.

Funding

Program 973 (2014CB921301); National Natural Science Foundation of China (NSFC) (11674117); Natural Science Foundation of Hubei Province (2015CFA040).